Absolute *pp*-elastic cross sections from 492 to 793 MeV

A. J. Simon and G. Glass*
Texas A&M University, College Station, Texas 77843

M. W. McNaughton and T. Noro†
Los Alamos National Laboratory, Los Alamos, New Mexico 87545

K. H. McNaughton and P. J. Riley
University of Texas, Austin, Texas 78712

E. Gülmez‡ and C. A. Whitten, Jr.
University of California, Los Angeles, California 90024

V. R. Cupps§ and R. D. Ransome
Rutgers University, New Brunswick, New Jersey 08903

D. L. Adams
Rice University, Houston, Texas 77251
(Received 25 March 1993)

Absolute *pp*-elastic-differential cross sections were measured at incident energies 492, 576, 642, 728, and 793 MeV from about 30° to 90° c.m. The total uncertainty was determined to be less than 1%, made possible by particle counting for beam normalization and extensive cross-checks of systematic effects. These new data are consistent with previous data above 600 MeV but have uncertainties about a factor of 10 smaller. Near 500 MeV these data are consistent with 90° data from TRIUMF, but differ significantly from similar data from PSI; the cause of this discrepancy is discussed.

PACS number(s): 25.40.Cm, 25.10.+s

I. INTRODUCTION

Proton-proton (*pp*) elastic scattering is fundamental to nuclear physics both as a test of strong-interaction theories and as basic input to microscopic models of the nucleus. The scattering amplitudes are usually derived from a phase-shift analysis (PSA) which interpolates between and smooths the discrete data points. The *pp*-elastic-differential cross section is an essential foundation for this analysis. The cross section σ enters the phase-shift analysis through the fact that the product $\sigma(\theta)X$ is equal to a bilinear combination of amplitudes, where X is some spin observable [1]. Hence, our knowledge of the phase shifts and amplitudes depends critically on how well the *pp* cross section is measured.

Furthermore, the inelasticities in the phase shifts are not well determined. The total inelastic cross section may be calculated as the difference between the total and elastic cross sections, and since the total cross section is well known to about 1% [2–4], knowledge of the elastic cross section will provide the information needed to arrive at the total inelastic cross section.

Many nuclear cross sections are normalized directly or indirectly to the *pp*-elastic cross section, especially in experiments where it is difficult to determine the beam normalization with calibrated ion chambers or Faraday cups. This provides additional motivation for precise *pp* measurements.

Previous measurements of the *pp*-elastic cross sections are inconsistent, disagreeing beyond the published uncertainties. The best way to determine systematic errors is to measure each quantity in several ways that are as different and independent as possible. The present experiment was designed with independent checks of all anticipated systematic errors in order to keep the total uncertainty well below 1%.

II. PREVIOUS EXPERIMENTS

A. Previous absolute cross-section data

There have been many measurements of the *pp*-elastic differential cross section, yet this cross section is not well determined. We benefited by studying these attempts and learned from previous experience. Conversely, our

*Present address: University of Texas, Austin, TX 78712.
†Present address: Osaka University, Research Center for Nuclear Physics, 10-1 Mihogaoka, Ibaraki, Osaka 567, Japan.
‡Present address: Boğaziçi University, Bebek, İstanbul, Turkey.
§Present address: Fermi National Accelerator Laboratory, Batavia, IL 60510.

experience enables us to identify weaknesses in some of the previous experiments. Therefore previous data are summarized in Table I and discussed below.

Many differential cross-section measurements are relative, not absolute; i.e., they are normalized to other data or to a phase-shift analysis (PSA). This is not always obvious from the publications. For example, the data of Albrow *et al.* [5] were entered into the database as absolute, but were in fact normalized to a PSA. The data of Garçon *et al.* [6] were entered as absolute, but are normalized to the Saclay PSA. The forward-angle data of Aebischer *et al.* (CERN, 1976) [7] were normalized to a PSA. The data of Hoffman *et al.* (LAMPF, 1988) [8] were entered as absolute, although they are normalized to the TRIUMF data of Ottewell *et al.* [9] (p. 398 of Ref. [8]).

The major difficulty with an absolute cross-section measurement is the absolute measurement of the number of beam particles. Barrett *et al.* [10] investigated the problems of beam normalization at LAMPF and reported on the construction of three devices: a Faraday cup, a secondary emission monitor, and an ion chamber. Only the Faraday cup is absolute, and this may in principle be used to calibrate the others.

Willard *et al.* [11] used this Faraday cup to measure absolute cross sections at 647 and 800 MeV. One of the present authors (M.W.M.) joined Willard's group just after this experiment. In this experiment the live time was measured with an Ortec 439 current integrator in coincidence with the electronic busy signal. Subsequent tests showed that the digitized pulses from the Ortec 439 are delayed so that they often occurred after the end of the LAMPF macropulse (which was 500 μs at the time). As a result the live time was seriously overestimated, which leads to cross-section values that are too low. The error is more serious at forward angles where the event rate was large. Further details are contained in a thesis ([12], pp. 49–50). These data are now omitted from most PSA's.

Irom *et al.* [13] used this same Faraday cup at LAMPF for absolute measurements from 3° to 15°. In Irom's thesis [14] he quotes verbatim from the design report [10] to justify his estimate of 3% uncertainty. One of the present authors (M.W.M.) was responsible for this Faraday cup at the time, and it is his opinion that the performance of the Faraday cup was better described in the words of the designers and builders (Ref. [11], Sec. III A): "We were troubled with charge leakage in the co-axial cables which increased the uncertainty ... to 10% in the worst case." At the time of the measurement of Irom *et al.* the Faraday cup had deteriorated further, which probably accounts for why these data are about 7% larger than the present PSA's.

Nikitin *et al.* (Moscow, 1955) [15] measured the cross section at 660 MeV with 5% statistics, using an ion chamber which was normalized to a Faraday cup. They quote 2% uncertainty for the Faraday cup and 4% uncertainty in the solid angle. These data are in good agreement with the latest data.

Ottewell *et al.* [9] used a Faraday cup at TRIUMF to measure absolute cross sections at 90° c.m. from 300 to 500 MeV with a quoted uncertainty of 1.9%, which does not include an estimate of the uncertainty of the Faraday cup. They obtained good internal consistency, but state (p. 191) that "it was assumed that all the beam charge was detected by the Faraday cup." Any loss of charge would lead to cross sections that are too large. These data are about 2% larger than the new data reported here.

Ottewell *et al.* [9] also tried counting the beam, following the method of Chatelain *et al.* (PSI, 1982) [16]. However, both publications overlook the effect of beam-intensity fluctuations. Chatelain *et al.* discuss Poisson statistics (p. 648), but the Poisson formula is nonlinear, so that in the presence of intensity fluctuations the average is biased. This bias is always in one direction, leading to an underestimate of the beam and therefore cross-section values that are too large. This appears to be the problem with the one data point obtained with beam counting by Ottewell *et al.* and also with the data of Chatelain *et al.* (The beam-intensity fluctuations are a result of beam motion on slits such as those described by Chatelain *et al.* on p. 644. The paper does not mention corrections for brief beam-off intervals.) In designing our present experiment we benefited from these previous experiences and kept the beam intensity low. This serious problem is discussed in more detail in Sec. II B.

TABLE I. Differential cross-section measurements from 450 to 900 MeV. Columns 1 and 2 give the energy and angle range, columns 3 and 4 give the typical point-to-point and normalization uncertainty, and column 5 suggests a renormalization relative to other data. An asterisk after a number indicates that Sec. II contains significant comments on this value.

Energy (MeV)	Angle (deg)	Uncert. (%)	Norm. (%)	Renorm. (%)	Ref.
450	90	1	2	0	[9]
516–582	90	1	1*	+3	[16]
501–832	34–86	6	3*	−10	[23]
460–657	30,90	7	0	0	[28]
516–857	22–89	10	0	0	[18]
470–873	23–90	10	5	−10	[20]
647,800	23–90	3*	4*	−10	[11]
650	6–90	20	3	0	[19]
660	30–90	4	4	0	[15]
648–992	7–17	2	5	0	[30]
648–995	4–10	10	5	0	[29]
665–831	51–89	11	9	−10	[21]
831	48–90	3	7	+10	[22]
582	15–90	2	*		[27]
529–582	30–90	1*	rel		[33]
285–572	4–22	2	rel		[7]
335–1958	40–90	7	rel		[5]
440–1000	30–90	2	rel		[25]
508–1203	90	2	rel		[6]
497.5	6–90	2	rel		[8]
796*	6–90	1*	rel		[34]
796*	3–15	1	3*	+7	[14]
796*	1–11	3	5	+9	[17]

Pauletta *et al.* (LAMPF, 1983) [17] counted the beam by placing the LAMPF high-resolution spectrometer (HRS) in the beam and quoted 5% normalization uncertainty for the data in Table I of Ref. 17 (3°–10° c.m. at 800 MeV). We benefited from their experience and used fast (300 MHz) electronics and fast (1 ns rise time) photomultipliers and scintillators (which were not available in 1982). This enabled us to resolve the 5-ns LAMPF microstructure. The data of Pauletta *et al.* are about 10% larger than present PSA's, most likely as a result of failing to account for all the particles in the beam.

Shimizu *et al.* (KEK, 1982) [18] counted the beam, but with a bubble chamber at low rates; consequently, the counting statistics are typically 10%. Similarly, Guzhavin *et al.* (1965) [19] used a bubble chamber and reported 20% statistical uncertainty.

Ryan *et al.* (PPA, 1971) [20] normalized by counting the beam in the spectrometer, but do not mention Poisson statistics. The statistical uncertainty of the data of Ryan *et al.* is about 6–10%. Williams *et al.* (Rutherford Laboratory, 1972) [21] also counted the beam and quoted a 9% normalization uncertainty. Kammerud *et al.* (ZGS, 1971) [22] counted the beam and quoted 7% normalization uncertainty. Abe *et al.* (ZGS, 1975) [23] counted the beam and quoted a 3% normalization uncertainty, but several authors [4,18,24] have pointed out that these data, if correct, would contradict dispersion relations. The data of Abe *et al.* are about 10% lower than other data.

Chatelain *et al.* [16] include the data of Smith, McReynolds, and Snow (BNL, 1955) [25] for comparison with Fig. 2 of Chatelain *et al.*, but Smith, McReynolds, and Snow normalized to the results of Sutton *et al.* at their overlap energy of 437 MeV. Sutton *et al.* (Carnegie, 1955) [26] normalized to an ion chamber, with the assumption that the calibration at 440 MeV was the same as the measurements by Chamberlain *et al.* at 345 MeV.

Boschitz *et al.* (SREL, 1972) [27] normalized to the activation reaction $^{12}C(p,pn)^{11}C$. It is not clear, however, what the absolute uncertainty is, especially as the publication referred to by Boschitz *et al.* is itself a relative measurement, with only a brief mention of absolute normalization.

Mescheriakov *et al.* [28] normalized to an ion chamber which was calibrated by a determination of the charge collected in a "massive proton absorber." These data agree with more recent data within the 7% uncertainty.

Velichko *et al.* (Leningrad, 1982) [29] used the IKAR ionization chamber to measure small-angle cross sections (5°–8° or 10°) with 10% statistical uncertainty. Dobrovolsky *et al.* (Leningrad, 1983) [30] also used IKAR, extending these measurements to 17°, with an estimated uncertainty of 2%.

With so much previous data it may be surprising that more data are needed. To summarize, there are forward-angle data and data near 500 MeV at 90° c.m., which claim accuracies of a few percent, but which disagree with each other sometimes by several standard deviations. At higher energies and backward angles, the uncertainties are closer to 10%. These results are summarized in Table I.

B. Pitfalls with beam counting

We suspect that the careful measurements of Chatelain *et al.* of the absolute cross sections from 516 to 582 MeV are a few percent high as a result of beam-intensity fluctuations caused by beam motion on slits. These cause the estimate of the number of beam protons to be low, because Poisson statistics is nonlinear. Since our present experiment also counted the beam, and since there is a serious disagreement between our data and the data of Chatelain *et al.*, it is important to clarify this.

The corrections of Chatelain *et al.* from Poisson statistics are exact if the beam rate is constant. If the rate fluctuates, then Chatelain *et al.* average a nonlinear function, resulting in a beam count that is always low. For example, a Poisson distribution $P = a^n e^{-a}/n!$ with a=0.4 combined with a distribution with a=0 is not equivalent to a distribution with a=0.2. If the rate fluctuates from zero to 0.4 proton/pulse, averaging 0.2 proton/pulse, then, by assuming that a=0.2, the method of Chatelain *et al.* undercorrects for the occurrence of two or more protons in one beam pulse. This example results in an estimate of the beam that is 3.3% too low, and therefore cross sections that are 3.3% too high.

Gülmez *et al.* [31,32] describe the method used in our present experiment in which we measured a series of delayed coincidences between successive beam pulses. In the presence of pulse-to-pulse fluctuations our method is no better than that of Chatelain *et al.*, giving identical results at the same beam intensity. However, if the beam fluctuation is slow compared with the coincidence delays, then our method is good. The results shown by Gülmez *et al.* demonstrate that our method gives cross sections about 1% too high for beam rates of 0.2 proton/pulse. Note that this source of error must always give cross-section measurements that are too high.

We believe that the only solution to this problem is to keep the beam rate low and to examine the measured cross section as a function of rate. Except for test runs, we used a rate near 0.01 proton/pulse, for which we estimate the error to be less than 0.1%. This is confirmed by comparison of the cross-section values obtained (at each angle and energy) for high, medium, and low beam rates (typically 0.03, 0.01, and 0.001 proton/pulse) as discussed below.

C. Previous relative cross-section measurements

Three relative measurements need to be discussed since they affect the phase-shift analysis.

Berdoz *et al.* [33] measured the relative cross section at 529, 556, and 582 MeV with statistical uncertainties of about 0.3%. Estimates of the systematic errors are in the text and must be combined with the statistical errors listed in the table. The beam energy significantly affects the shape of the angular distribution so that the 1.5 MeV uncertainty contributes about 0.4% to the cross-section uncertainties. Other systematic errors contribute 0.3–0.6%.

Barlett *et al.* [34] measured the relative cross section at LAMPF near 800 MeV. Their table lists 70 points

from 6° to 90° c.m., each with a statistical uncertainty of 1%, but there is no estimate of the systematic errors. Similarly, Pauletta *et al.* [17] list 86 points from 1° to 11°, also with no estimate of systematic errors.

The multiwire drift chambers (MWDC's) used in these LAMPF measurements were almost identical to the MWDC's that we used as monitor detectors (Sec. III D). As Barlett *et al.* discuss on p. 688, these wire chambers have a typical efficiency of less than 90%, which is rate dependent and is higher in the center than near the edges. Barlett *et al.* measured the relative efficiency (p. 688) and suggested that this leads to a point-to-point uncertainty of 1–3 % (p. 690). In addition, there is the problem of monitoring the relative beam intensity from one angle setting to the next. On pp. 689–690 they state that the primary and backup ion chambers tracked to 1.5% and conclude that this leads to a systematic error of less than 1%.

These same uncertainties are discussed by Hoffmann *et al.* [8] and summarized in Table I and near the end of p. 398, with the conclusion that the point-to-point systematic errors are about 2%. After discussion with the principal authors we conclude that 2% is a reasonable estimate of the point-to-point systematic uncertainty at both 497 and 800 MeV, and should also be applied to the data of Barlett *et al.* [34] and Pauletta *et al.* [17].

Two other items need to be clarified. First, the beam energy is more likely to be 796 MeV rather than 800 MeV (see Sec. III A below). Second, although a 2% normalization uncertainty is mentioned by Hoffmann *et al.* [8], these data are not absolute, but were normalized to the data of Ottewell *et al.* [9].

III. EXPERIMENTAL METHOD

A. Accelerator and beam energy

This experiment was performed with the external-proton (EP) beam line at the Clinton P. Anderson Meson Physics Facility (LAMPF). Data were obtained at five nominal proton beam energies: 496.7, 581.6, 648.3, 733.4, and 797.0 MeV. Three of these energies were measured during some of our data runs using the high-resolution spectrometer (HRS) and were found to be 581.1, 647.0, and 798.0 MeV with an uncertainty of ±0.5 MeV.

Values for the beam energy were also obtained from the beam-line magnets. The 581.1- and 647.0-MeV settings of the beam-line magnets scaled by a factor 1.0692 ± 0.0004, where the uncertainty is the standard deviation from several beam lines. This is almost exactly the expected ratio of the momenta. For the 497-MeV setting, the beam-line magnetic fields were reduced by a factor 0.9097 ± 0.0008, from which we calculate the energy 497.8 ± 0.7 MeV. At 733 MeV there was no user in the adjacent beam lines, and so a major beam-line component (LBSO) was off; furthermore, the tuning was poor at the exit from the accelerator; so only two magnets scale sensibly. From these we calculate the energy to be 735 ± 2 MeV.

The energy of the beam at LAMPF varies from time to time depending on the quality of the tuning, but is generally believed to be stable to about ± 1 MeV. On two occasions (not simultaneous with this experiment) the LAMPF beam energy was measured using the long neutron time-of-flight (NTOF) neutron flight path. Results were 494.3 ± 0.6 MeV for the nominal 496.7-MeV setting and 795 ± 1 MeV for the 797-MeV setting. However, the 797-MeV setting is believed to be controlled to 797 ± 1 MeV by the requirements of the proton storage ring (PSR) at LAMPF. For the 494.3-MeV measurement the uncertainty does not include the effect of the rebuncher that is used by the neutron time-of-flight experiment at this energy; this could account for the 2-MeV energy shift.

From time to time, energy measurements have been reported from the LAMPF high-resolution spectrometer (HRS). Hoffmann *et al.* [8] reported 497.5 ± 0.5 MeV for the nominal 496.7 MeV. Irom (Ref. [14], p. 50), Bevington *et al.* [35], and McNaughton *et al.* [36] all reported measurements of 796 ± 2 MeV for the nominal 797 MeV.

The most precise measurements of the LAMPF beam energies have been made by observing resonances in the photodetachment cross section of H^0 [37,38]. For the 797-MeV setting, they report two measurements: $\beta = 0.84103 \pm 0.00007$ for the unstripped H^- beam, which corresponds to 797.0 MeV for the H^- beam, and 796.1 ± 0.3 MeV for the stripped protons, and 0.84109 ± 0.00002, which gives 796.4 ± 0.1 MeV for the protons.

In the analysis of this experiment, we assumed beam energies of 497.8, 581.1, 647.0, 733.4, and 798.0 MeV. These are the measured values for four of the energies and the nominal value for 733.4 MeV. These were corrected for energy losses in the materials between the evacuated beam line and the target center. The energy loss in the full 19.75-cm LH_2 (liquid hydrogen) target ranged from 6.6 to 8.0 MeV, and so the measurements reported here are averages over ±3 to ±4 MeV. The energies at the LH_2 target center were 491.9, 575.5, 641.6, 728.2, and 793.0 MeV, with an uncertainty of ± 1 MeV. The estimated uncertainty of ± 1 MeV is the standard deviation between the nominal and the measured beam energies for the various measurements discussed above.

B. Beam

Although this was an unpolarized measurement, a Lamb-shift polarization source was used to initiate the proton beam. A longitudinally polarized beam (L spin) was generally used in order to avoid the complication of polarization asymmetry. Residual vertical components were less than 0.01 in magnitude. These were measured by either of two beam-line polarimeters, and unwanted asymmetries were canceled to better than 0.1% by flipping the beam spin every 2 min and calculating an unweighted average for the two polarization states. Occasionally, a vertically polarized beam (N spin) was used for systematic checks (Sec. III G).

The accelerated beam particles were H^- ions. These passed through a small (few mm) aperture in a stripping foil (LBST1) before being stripped to H^+ (protons) by a 3-μm plastic foil (EPST0) between two bending magnets (EPBM1 and EPBM2). This arrangement elimi-

nated beam contamination since any beam particle with a different momentum or whose charge did not change from minus to plus at the stripper was swept aside by the magnets. Finally, the aperture in the LBST1 stripper was focused onto the target by quadrupole magnets, to give a clean beam spot (free of beam halo) a few mm in diameter. We calculate the beam halo outside the target and beam counters to be less than 0.1%. This was empirically confirmed by examining the histograms of the interaction points at the target and by comparing results with the beam counters in and out of coincidence to check for a beam that might have missed these counters. Typical beam divergence was about 0.1 mrad. The beam spot was continually monitored to ± 1 mm with an insertable strip ion chamber (EPII5).

Most of the data were taken with a beam bunch spacing of 5 ns (accelerator rf: 201.25 MHz). Some data were taken with the 100-ns spacing produced by the 10-MHz buncher and chopper. This provided a valuable check on the beam-counting system (Sec. III C).

C. Beam counting

One major difference between this experiment and many previous measurements of the *pp* differential cross section is the way the absolute normalization of the beam was determined. Many previous experiments used Faraday cups or ion chambers, or relied on previous experiments for a normalization factor. This experiment made use of a particle-counting method for the determination of the beam intensity [31,32]. The two major sources of possible systematic error are (1) multiple protons in a single beam pulse (or rf beam bucket) and (2) attenuation by material in the beam.

Three thin (1 mm), circular (38 mm in diameter) scintillators made of Bicron BC418 plastic (0.5 ns rise time) labeled B1, B2, and B3 (Fig. 1) were placed in the beam at 0.8, 0.7, and 0.6 m upstream of the target. The efficiencies were measured by several methods that used different combinations of beam and scattered proton detectors. If the beam counters are included in the requirements for the scattered proton yield, then their efficiencies cancel from the cross-section calculation. This procedure is equivalent to the scattered proton detectors being used to measure the beam-counter efficiency. All methods were consistent to better than 0.1%. The beam-counting scintillators were generally greater than 99.5% efficient when taken separately. However, taken as a majority of two of three, the efficiency was better than 99.99%.

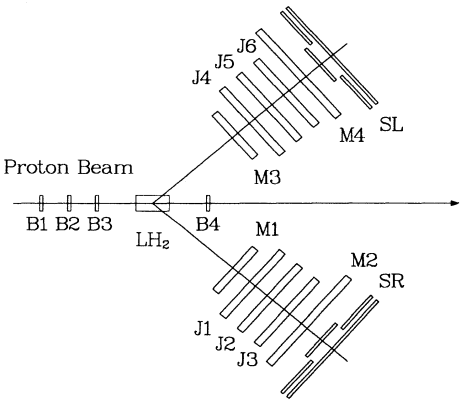

FIG. 1. Experiment layout. B1–4 are beam scintillators, SL and SR are scattered particle scintillators, M1–4 are MWPC's, and J1–6 are MWDC's.

The scintillators were connected to Hamamatsu R2083 photomultiplier (PM) tubes and H2431 bases with 0.7 ns rise time. In order to ensure that signals from neighboring bunches (5 ns apart) did not overlap, the output of each PM tube was clipped with a 10-cm, 50-Ω RG223 coaxial cable terminated by a 27-Ω resistor. These signals were transmitted to the counting house electronics via low-attenuation (SLA 12–50 J) coaxial cables in order to preserve their high-frequency components. The signals were processed by an innovative electronic system [31] using Phillips 704 and 754 electronic modules, which were tested at 300 MHz.

The pulse-height spectra were clean. At high rates, a second peak at twice the pulse height was observed, resulting from events in which two protons passed through the counters. This was not quantitatively useful, however, partly as a result of the Landau tail and partly because it was difficult to gate the analog signal at 200–300 MHz.

Extensive tests on the system have been described in detail [31]. At each of the five beam energies the system was tested and it was verified that adding or subtracting 1 ns of delay made less than 0.1% change to the data. At every angle setting, data were recorded at high, medium, and low rates, covering a range of about a factor of 10 in rate, and it was verified that the results were consistent within counting statistics. Gülmez *et al.* [31] have demonstrated that the beam-counting system is stable to 0.1% over more than a factor of 100 in rate and is stable within the counting statistics up to 0.1 proton/pulse. Most of the data were obtained with beam rates near 0.01, but with test runs near 0.1 or 0.001 proton per pulse.

A fourth scintillator B4 (51 mm diameter) was placed downstream of the target to measure beam attenuation by the target, air, and beam counters. The position of B4 ranged from 0.3 to 1.2 m from the target. Calculations for absorption were made with the known [39,40] proton-proton and proton-carbon total cross sections and a knowledge of how much material (z) was in the beam path. In regions where the pC cross section is not well known, the nC total cross section was substituted. The correction factor for each material is $\exp(-\sigma_T z)$. These are multiplied together to give the products shown in Table II. In Table II the calculations for the full target length are compared with the measured attenuation using B4. The corrections applied to the cross sections correspond to half the target length and are therefore approximately the square root of these values.

The beam attenuation corrections were further checked by the insertion of dummy targets, plastic scintillators, and vacuum windows and the remeasurement of the at-

TABLE II. Beam attenuation corrections to the target center. Also listed are calculated compared with measured transmissions through the full target.

Nominal energy (MeV)	Correction	Calc. trans. at B_4	Measured trans. at B_4
497	0.981	0.956±0.001	0.958±0.001
581	0.978	0.958±0.001	0.959±0.001
647	0.977	0.955±0.001	0.955±0.001
733	0.975	0.948±0.001	0.950±0.001
798	0.973	0.947±0.001	0.947±0.001

tenuation with the B4 detector to verify that the attenuation for each of these materials scaled as expected. All these data were consistent within the estimated uncertainty of 0.001.

D. Detectors

Two identical detector arrays were placed on either side of the beam line to detect both scattered protons (see Fig. 1). Each array contained detectors of three different types: scintillator hodoscopes, multiwire drift chambers (MWDC's), and multiwire proportional chambers (MWPC's). The resulting redundancy provided many consistency checks on possible systematic errors.

Each array consisted of seven items, spaced about 10 cm apart (Fig. 1), as follows: front MWPC, three MWDC's (J1, J2, and J3 on the right and J4, J5, and J6 on the left), back MWPC, two scintillator hodoscope planes.

Each scintillator hodoscope was made of two planes, an X plane made of three vertical detectors 305 mm wide by 610 mm high by 6 mm thick and a Y plane made of four horizontal detectors 864 mm wide by 216 mm high by 5 mm thick. The event trigger required coincident signals from at least three of the four scintillator planes.

Gülmez *et al.* [41,42] used this same equipment to measure absolute cross sections for pd elastic and $pp \rightarrow d\pi$. In these experiments, the scintillator pulse height was used to distinguish between p, d, and π. For pp elastic, the signal was so clean that the scintillator pulse height made no difference, and so it was ignored in the final analysis (Sec. IV).

The front MWPC's were 512 mm wide by 384 mm high with 2 mm wire spacing. The back MWPC's were 816 mm wide by 624 mm high with 3 mm wire spacing. Individual amplifiers on each wire and an encoding system [43,44] were used to read every hit wire and transfer the data to the on-line computer, thus ensuring high efficiency without loss of multiple-hit events. Events with more than one wire hit in an MWPC were reconstructed using the redundancy provided by eight MWPC planes.

The MWDC drift chambers, placed between the MWPC's, were 580 mm by 580 mm with 0.2 mm resolution. Their primary role was to check the geometry and monitor the efficiency of the other detectors.

The detector arrays, attached to telescoping radius arms, were pivoted to cover angles from 10° to 80° laboratory and ranged in radius (to the front MWPC) from 0.4 to 1.4 m. Angular coverage at a single setting was typically 20°. Five angular settings usually covered the full angular range, allowing a generous overlap to check systematic errors.

E. Efficiency

Because of their higher efficiency (typically 99.9% per plane), the MWPC's as opposed to the MWDC's were used to measure the scattering yield into a given solid angle. The three MWDC's were placed between the two MWPC's to check the geometry and to determine the efficiency of the MWPC's.

Six different methods [40] were used to measure the efficiency of the MWPC's, and the uncertainty was estimated from the internal consistency of these methods. In all cases, good pp-elastic events were determined by various combinations of MWPC's or MWDC's and used to test the efficiencies. In one method, seven of the MWPC's were used to test the eighth. In several methods the MWDC's were used to test the MWPC's, both singly and in combinations, for each angle bin.

Typically, the efficiency of the product of all eight MWPC planes was 99%, with most of the inefficiency traceable to two bad wires in one plane. The efficiency was measured separately for each scattering-angle bin with an uncertainty of 0.2%.

Hodoscope scintillator efficiencies were generally 99.9% taken individually. However, since the trigger was a requirement of three of the four planes, the total efficiency was greater than 99.99%.

F. Live time

The live time of the on-line computer and data-acquisition system was measured by four different methods, with a variety of fast scintillator combinations that had rates proportional to the beam or event rate, to sample the electronic busy signal. In addition, raw hodoscope triggers were scaled and compared with the triggers recorded by the on-line computer. Agreement among these methods was taken as an estimate of the uncertainty in the live time. Typical uncertainty was 0.1%.

As a stringent test of the live-time corrections, data were recorded with live times ranging from 20% to 99%. For every angle and energy setting, data were recorded for three rates: low, medium, and high, corresponding to live times of greater than 90%, 80%–90%, and 70%–80%. Occasional very high rate runs were made with live times as low as 18%. The cross sections calculated from each case were internally consistent within their combined statistical accuracy of 0.1%.

G. Geometry

The chambers were aligned and their placement determined with standard surveying equipment. The same instruments were used to determine both the chamber separation and the wire spacing, and so equipment calibration errors cancel from the solid-angle determination.

In some cases, when the wire spacing was not uniform, tables of the wire spacing as a function of position were used. The measurements were cross-checked by a detailed examination of internal consistency [40] using the redundant information obtained from the MWDC's, which provided five X points and five Y points for every proton track. The uncertainty in the wire spacing was typically 0.03%, contributing 0.2% to the uncertainty in the solid angle.

Chamber separation was measured by four different techniques and cross-checked with the MWDC's using the redundancy of five points to define a line as above. Parallel tracks verified the wire spacing, while diverging tracks verified the chamber separation. The uncertainty in the separation was estimated to be 0.07% for the left arm and 0.12% for the right arm, mostly as a result of bowing and twisting of the chamber frames.

It was difficult to locate individual wires in a sealed chamber, but nevertheless, the direct measurements of the absolute scattering angle θ were accurate to $\pm 0.1°$ laboratory. These were improved with a measurement [42] of the maximum deuteron angle from the reaction $pp \to d\pi$ and also from the asymmetry for $pp \to pp$ at 90° c.m. with a normally polarized beam. The maximum deuteron angle is accurately known from $pp \to d\pi$ kinematics. The angle at which the $pp \to pp$ asymmetry passes through zero is required to be 90° c.m. by the identity of the two scattered protons. All these measurements were consistent with our estimated uncertainty of $\pm 0.04°$ laboratory, with the exception of the measurements near 28° laboratory at 728 MeV, for which we made a 0.06° correction and increased the uncertainty to 0.07° laboratory.

Two additional checks on the geometry were obtained as follows. First, cross sections were extracted near 90° c.m. with only the left arm or only the right arm to determine the solid angle. The ratio (left/right) was 1.004 ± 0.001, where the uncertainty is statistical only. This is consistent with our estimate of the systematic uncertainty in the solid angles: 0.2% for the left arm and 0.3% for the right arm. Most of this 0.4% discrepancy between left and right arms probably results from distortion of the right-arm wire chambers; since the left arm was used to define solid angle for most of the data, this 0.4% discrepancy represents the worst case.

Also, the overlap between the angular settings allowed us to measure the same cross section using first the large-angle side and then the small-angle side of the detector. The ratio of the two measurements was 1.003 ± 0.001, where the uncertainty is statistical only. This result indicates a systematic error of 0.3%, which is either from the solid angle $\Delta\Omega$ or from the scattering angle θ and is consistent with our uncertainty estimates.

H. Hydrogen target

Solid targets as well as a liquid target were used in this experiment. The liquid-hydrogen (LH_2) target was used to record the bulk of the data for the cross-section measurement. CH_2 targets of two different densities and several thicknesses were used to check target thicknesses, scattered particle absorption corrections, and background subtraction.

1. Liquid hydrogen

The liquid-hydrogen target was especially designed to avoid systematic errors in the effective target thickness. The liquid was contained in a cylinder 197.5 mm in length and 54 mm in diameter. An inner cylinder, 43 mm in diameter, deflected hydrogen bubbles that could be created near potential heat sources on the outer cylinder and kept them from entering the beam-target interaction region. Beam heating, typically 10^{-7} W, was negligible. To maintain flat end windows, the LH_2 target was contained within a flask of cold hydrogen gas at the same pressure as the liquid. The gas flask was 360 mm in length and 136 mm in diameter with hemispherical end caps. It was insulated with 20 layers of 6-μm-thick aluminized Mylar and was surrounded by an insulating vacuum. "Hydrostatic" pressure from the weight of liquid hydrogen caused a small pressure differential, causing each end window to bow out by 0.28 mm.

Target pressure and temperature were continuously maintained and monitored using three calibrated gauges and ten temperature-sensitive diodes. A target temperature of 19.87 ± 0.03 K (20.13 ± 0.10 K for 492 MeV) was maintained during the full target runs, which corresponded to a target density of 0.07121 ± 0.00003 g/cm^3 (0.07095 ± 0.00007 g/cm^3 for 492 MeV). When cold, the target could be emptied and refilled within an hour, and the target was emptied periodically for data collection to be used in target-length measurements. A catalytic converter was also used to speed the conversion from ortho-hydrogen to the equilibrium para-hydrogen. The densities of ortho-LH_2 and para-LH_2 are different by 0.6% at these temperatures.

The target length was measured in three different ways: a physical measurement with standard surveying equipment and two methods that used target traceback information from the MWPC detectors. The length recorded from the physical measurement was 197.7 ± 0.2 mm with the empty target at room temperature. The target was filled with alcohol to detect possible distortions in the end windows due to hydrostatic pressure. The result was a 0.32% increase in length, which was in good agreement with a calculated value of 0.31%. For liquid hydrogen, the correction is 0.28%. After a correction factor of 0.6% was included for the contraction of Mylar at liquid-hydrogen temperatures, the target length was determined to be 197.1 ± 0.2 mm.

The other two target-length measurements made use of target traceback from the MWPC's. The point of closest

approach at the target was calculated from the two rays for a good *pp*-elastically scattered event and the X, Y, and Z positions of the struck proton were deduced for both empty and full targets.

Empty-target measurements were made at each energy and several angle settings for the detector arrays. Two peaks, which corresponded to the LH_2 target end caps, were easily distinguishable in histograms of the target traceback. The separation of the centroids of these peaks was taken as the target length. It is not known whether the windows retain some of their distortion when the target is emptied, and so a correction factor of 0.14% was used, giving a corrected length of 198.0 ± 0.2 mm.

For a full target, Monte Carlo calculations showed that the best value for the target length was the half-height width of the distribution. The average for the full targets was 197.3 ± 0.2 mm.

The 0.2-mm uncertainty for each case represents the internal consistency for that case. The best estimate for the target length was taken to be 197.5 mm, with an uncertainty of 0.5 mm estimated from the consistency of these three methods.

The effective target thickness (protons/unit area) for the cross-section calculations included the hydrogen in the two 0.08-mm Mylar end windows (a 0.1% correction) and the hydrogen gas included in the target traceback cuts (a 0.3% correction).

2. CH_2 targets

To check the hydrogen-target thickness, data were taken with a variety of CH_2 targets, and the results were compared with those from liquid hydrogen. Sixteen samples of low-density CH_2 and four samples of high-density CH_2 were prepared, and cross sections were measured using these in various orientations so as to expose different sections of the same target to the beam. Thicknesses ranged from 13 to 52 mm.

Sundqvist *et al.* [45] investigated the effective thickness of CH_2 targets and concluded that the uncertainties from CH_3 clusters and from contamination were less than 0.2%. We compared two grades of CH_2, low density and high density. The ratio of the cross sections measured with these two materials (low/high) was 0.997±0.004.

The CH_2 target densities were (0.9197 ± 0.0007) g/cm^3 and (0.9679 ± 0.0006) g/cm^3. The uncertainties represent the standard deviation of many measurements of different samples. Uniformity was checked by using several samples in different orientations so as to expose different sections to the beam. No significant differences were found. Each sample was exposed to about 10^9 beam protons, and so the loss of hydrogen was negligible, as was confirmed by examining the data as a function of exposure time.

The ratio of the cross sections measured from CH_2 to those from liquid hydrogen was 1.004 ± 0.005, where the error includes the systematic uncertainties, which are dominated by attenuation (0.3%, Sec. IV A) and background subtraction (0.3%, Sec. IV B). Near 492 MeV this ratio was 1.004 ± 0.004, which checks that the slightly different conditions of temperature and density for the LH_2 target at 492 MeV were measured correctly.

IV. ANALYSIS

The differential cross section can be written as

$$\sigma(\theta) = \frac{Y}{BT\Delta\Omega}$$

where Y is the number of particles scattered into a solid angle $\Delta\Omega$, B is the beam normalization factor, and T is the target particle density per unit area. The measurement of B was discussed in Sec. III C, T in Sec. III H, and $\Delta\Omega$ in Sec. III G.

The yield Y of elastically scattered protons was obtained by replaying the data recorded on magnetic tape. To avoid loss of good events and to minimize the corrections, the data were subjected to only four cuts as follows: (1) The trajectories of the two protons were traced back to their point of closest approach, and the z coordinate of this point was required to be within the target. (2) The scattering angle θ was used to define bins, typically 0.03 rad wide. (3) The azimuthal angle ϕ was limited to the acceptance of the detectors (from all points in the target), typically ± 0.15 rad. (4) The angular correlation θ and coplanarity $\Delta\psi$ were combined into a parameter RSQ and used to correct for background as described in Sec. IV B.

About 4% of the good events recorded more than one hit in one of the MWPC detectors. All hits were read into the computer, and the events were reconstructed with the redundant information in the eight MWPC planes. The reconstructed multiple-hit events were compared with events that had exactly one hit in every plane and were found to be consistent with the hypothesis that they were the result of electrons scattered from the air or plastic windows (δ rays). The uncertainty is included in the efficiency estimates (Sec. III E).

The yield Y was corrected for detector efficiency (Sec. III E), live time (Sec. III F), attenuation of scattered protons (Sec. IV A), background (Sec. IV B), and Coulomb multiple scattering (Sec. IV C).

A. Attenuation of scattered protons

About 1% of the protons that scattered from the target were displaced by a second scattering from hydrogen, carbon, or air before reaching the detectors. Since both scattered protons had to be detected, typical corrections were about 2%. This attenuation of the scattered particles was calculated with total cross sections for p carbon and pp. A Monte Carlo calculation determined the fraction of events that scattered both into and out of the cuts used to select good *pp*-elastic events.

As a check of this calculation, a large piece of CH_2 was inserted between the target and the detectors so that particles scattered from the target would have to pass through the CH_2 absorber to the detectors. Comparison between these runs and similar runs without the absorber

indicated that the effective pC cross sections are about 10% smaller than the values from Ref. [39]. Reduction of these cross sections by 10% also improved the internal consistency of the beam attenuation measurements (Sec. III C) and the results from different CH_2 target thicknesses. This probably results from some reaction products being detected as if they were continuing protons, as described in Ref. [46]. Consequently, we have used pC cross section that are 10% lower than Ref. [39] and assigned an uncertainty of 10% to this cross section.

B. Background

Background events for this experiment mostly came from proton-carbon quasifree scattering, the reactions $pp \to pn\pi^+$ and $pp \to pp\pi^0$. Some of these were eliminated by cuts on the kinematical quantities $\Delta\theta$ and $\Delta\psi$. $\Delta\theta$ is given by the difference of expected and observed angles:

$$\Delta\theta = \theta_e - \theta_o.$$

The angle θ_e is given by

$$\tan(\theta_e) = \frac{1}{(1 + T/2m_p)\tan(\theta_2)},$$

where θ_2 is the scattering angle of the second proton with respect to the beam, T is the incident beam energy, and m_p is the proton mass. The value $\Delta\psi$ is the coplanarity ($\phi_l - \phi_r$) angle multiplied by $\sin(\theta_l)$. (ψ is sometimes called the gunner's angle.) These two quantities $\Delta\theta$ and $\Delta\psi$ were combined quadratically to provide a single value RSQ from which the background was determined.

Chamber resolution and Coulomb multiple-scattering effects resulted in a distribution in the variable RSQ with a sharp peak near zero on a flat or smoothly decreasing background. The background shape due to these effects was simulated with a Monte Carlo program and compared with background data from a carbon target. The background spectra were normalized by fitting the tails (more than five standard deviations from the peak) and subtracted. With the LH_2 target the background correction was less than 0.3%, with an uncertainty of less than 0.1%. With CH_2 targets, the background was typically 5% with an uncertainty of 0.5%.

C. Coulomb multiple scattering

The total cross sections used for the corrections in Sec. IV A are for nuclear scattering, and therefore protons that Coulomb scatter between the target and the detectors must be included in the yield Y or otherwise corrected for. Event selection cuts on the angular correlations $\Delta\theta$ and $\Delta\psi$ (Sec. IV B) were usually more than 5 times the rms peak width, but Coulomb multiple scattering has a long tail, and so corrections were calculated and compared with the tails observed in the RSQ histogram (Sec. IV B). The uncertainty was estimated from the difference between the calculation and the observed tails after background subtraction. The uncertainty was less than 0.1% for the LH_2 data and less than 0.3% for the CH_2 data.

D. Displaced events

As discussed above we have corrected for events that are displaced from their proper kinematic locations by Coulomb scattering and by nuclear scattering. Events in which a secondary electron was scattered into a wire chamber resulted in extra wire hits being read into the computer and were corrected for by track reconstruction.

Using a Monte Carlo program we have examined other possible causes for displaced events, such as in- and outscattering from a particular angle bin, and we conclude that these corrections are less than 0.1%.

E. Errors

Systematic uncertainties for the LH_2 data are summarized in Table III. Whenever possible these uncertainties have been estimated from the standard deviation of several measurements as follows: (i) beam counting (0.1%, Sec. III C): measurements as a function of rate; (ii) beam attenuation (0.1%, Sec. III C): calculations and measurements including dummy targets; (iii) efficiency (0.2%, Sec. III E): redundant sets of chambers and six methods; (iv) live time (0.1%, Sec. III F): measurements as a function of rate using four methods; (v) solid angle (0.3%, Sec. III G): four measurement techniques, redundant sets of chambers, and overlapping angle settings; (vi) absolute angle (0.04°, Sec. III G): $pp \to d\pi$ kinematics and polarization at 90° c.m.; (vii) hydrogen targets (0.3%, Sec. III H): three measurement techniques and comparison of LH_2 with different thicknesses and densities of CH_2; (viii) scattered proton attenuation (0.2%, Sec. IV A): Monte Carlo calculation, comparison of LH_2 with CH_2, different thicknesses of CH_2, and dummy attenuator; (ix) background (0.1%, Sec. IV B): Monte Carlo calculation and comparison of LH_2 with CH_2.

Although it is an oversimplification, it is convenient to separate the systematic uncertainties into an overall

TABLE III. Summary of systematic corrections and uncertainties.

	Correction	Uncertainty
Beam energy		1 MeV
Beam counting		0.1%
Beam attenuation	2%	0.1%
Scattered attenuation	2%	0.1%
Efficiency	1%	0.2%
Live time		0.1%
Solid angle		0.3%
Absolute angle		0.04° lab.
Target thickness		0.3%
Background	1%	0.1%
Coulomb scattering	0.2%	0

normalization uncertainty, which affects all data equally, and point-to-point uncertainties. Thus the target thickness (0.3%) and average solid angle (0.3%) combine to give an overall normalization uncertainty, which has been rounded up to 0.5% since some of the point-to-point uncertainties are correlated. This normalization uncertainty applies equally to all data in Tables IV(a)–IV(e). Variation of the solid angle within a detector (0.3%) was taken as a point-to-point uncertainty. All of the other uncertainties were calculated individually for each data point. The uncertainties in cross sections corresponding to the uncertainties in beam energy and scattering angle were calculated from the phase-shift predictions and included in the combined point-to-point systematic uncer-

TABLE IV. *pp*-elastic-differential cross sections in the center of mass (c.m.) and laboratory (lab) systems. The total uncertainty (tot) includes both the statistical (stat) and systematic (sys) point-to-point uncertainties, which are listed separately as percentages. In addition the overall normalization uncertainty of 0.5% applies to all data equally in this table.

(a) *pp*-elastic cross sections at 491.9 MeV

$\theta_{c.m.}$	mb/sr	±tot	θ_{lab}	mb/sr	% stat	% sys
45.22	4.249	0.026	20.34	18.899	0.28	0.55
48.95	4.150	0.025	22.06	18.058	0.27	0.54
52.67	4.022	0.024	23.78	17.093	0.27	0.52
56.36	3.908	0.025	25.50	16.196	0.47	0.45
60.03	3.819	0.023	27.22	15.411	0.45	0.39
63.69	3.746	0.022	28.93	14.692	0.45	0.38
67.31	3.708	0.022	30.65	14.116	0.45	0.40
70.92	3.614	0.022	32.37	13.330	0.45	0.39
74.50	3.539	0.015	34.09	12.632	0.24	0.35
78.05	3.461	0.015	35.81	11.931	0.26	0.33
81.58	3.440	0.014	37.53	11.439	0.24	0.34
85.09	3.427	0.014	39.25	10.975	0.24	0.34
88.58	3.420	0.014	40.97	10.531	0.24	0.34

(b) *pp*-elastic cross sections at 575.5 MeV

$\theta_{c.m.}$	mb/sr	±tot	θ_{lab}	mb/sr	% stat	% sys
29.97	5.521	0.053	13.18	27.220	0.52	0.81
33.19	5.329	0.047	14.61	25.929	0.42	0.77
37.03	4.982	0.035	16.33	23.821	0.41	0.57
40.86	4.777	0.031	18.05	22.400	0.40	0.52
44.67	4.494	0.028	19.77	20.634	0.40	0.48
48.45	4.319	0.025	21.49	19.379	0.31	0.48
52.21	4.059	0.022	23.20	17.766	0.31	0.44
55.95	3.842	0.026	24.92	16.378	0.54	0.42
59.67	3.657	0.025	26.64	15.157	0.54	0.41
63.36	3.434	0.023	28.36	13.815	0.54	0.39
67.02	3.348	0.022	30.08	13.054	0.54	0.39
70.65	3.190	0.021	31.80	12.033	0.54	0.39
74.26	3.067	0.015	33.52	11.177	0.24	0.44
77.84	2.951	0.015	35.24	10.373	0.24	0.43
81.39	2.882	0.014	36.96	9.754	0.27	0.42
84.91	2.847	0.014	38.67	9.267	0.27	0.41
88.41	2.824	0.014	40.39	8.824	0.27	0.41

(c) *pp*-elastic cross sections at 641.6 MeV

$\theta_{c.m.}$	mb/sr	±tot	θ_{lab}	mb/sr	% stat	% sys
29.72	6.485	0.060	12.89	32.803	0.46	0.80
33.61	6.025	0.054	14.61	29.978	0.46	0.76
37.49	5.461	0.042	16.33	26.667	0.46	0.62
41.36	5.071	0.037	18.05	24.261	0.45	0.57
45.20	4.664	0.032	19.77	21.819	0.45	0.52
49.02	4.249	0.026	21.49	19.404	0.35	0.51
52.82	3.927	0.024	23.20	17.472	0.35	0.50
56.59	3.586	0.022	24.92	15.513	0.37	0.50
60.33	3.340	0.024	26.64	14.028	0.57	0.44
64.04	3.028	0.022	28.36	12.328	0.58	0.42
67.72	2.811	0.021	30.08	11.074	0.59	0.47

(c) *pp*-elastic cross sections at 641.6 MeV

$\theta_{c.m.}$	mb/sr	±tot	θ_{lab}	mb/sr	% stat	% sys
71.37	2.622	0.020	31.80	9.978	0.61	0.46
74.99	2.444	0.015	33.52	8.970	0.33	0.52
78.59	2.316	0.014	35.24	8.185	0.34	0.51
82.15	2.265	0.014	36.96	7.694	0.35	0.51
85.67	2.194	0.014	38.67	7.154	0.42	0.48
89.17	2.145	0.014	40.39	6.704	0.42	0.47

(d) *pp*-elastic cross sections at 728.2 MeV

$\theta_{c.m.}$	mb/sr	±tot	θ_{lab}	mb/sr	% stat	% sys
28.86	7.892	0.078	12.32	41.335	0.44	0.88
32.83	7.008	0.055	14.04	36.080	0.45	0.64
36.78	6.183	0.046	15.76	31.227	0.46	0.59
40.70	5.476	0.036	17.48	27.072	0.37	0.54
44.60	4.827	0.033	19.19	23.315	0.30	0.62
48.47	4.221	0.030	20.91	19.880	0.31	0.63
52.32	3.689	0.027	22.63	16.906	0.33	0.65
56.13	3.219	0.031	24.35	14.330	0.57	0.76
59.92	2.791	0.027	26.07	12.048	0.60	0.77
63.67	2.445	0.024	27.79	10.213	0.62	0.73
67.39	2.203	0.021	29.51	8.893	0.64	0.73
71.07	1.926	0.019	31.23	7.499	0.68	0.70
74.72	1.744	0.011	32.95	6.540	0.32	0.56
78.34	1.590	0.010	34.66	5.731	0.34	0.56
81.92	1.496	0.011	36.38	5.177	0.40	0.59
85.47	1.425	0.010	38.10	4.728	0.40	0.58
88.98	1.391	0.010	39.82	4.414	0.41	0.56

(e) *pp*-elastic cross sections at 793.0 MeV

$\theta_{c.m.}$	mb/sr	±tot	θ_{lab}	mb/sr	% stat	% sys
27.86	9.055	0.098	11.75	48.725	0.41	1.00
31.88	7.799	0.071	13.46	41.248	0.42	0.81
35.87	6.754	0.058	15.18	35.029	0.44	0.74
39.84	5.781	0.045	16.90	29.341	0.34	0.70
43.79	4.995	0.035	18.62	24.758	0.29	0.64
47.71	4.249	0.029	20.34	20.522	0.31	0.62
51.59	3.629	0.025	22.06	17.047	0.32	0.61
55.44	3.108	0.023	23.78	14.170	0.44	0.60
59.26	2.620	0.023	25.50	11.574	0.66	0.58
63.05	2.228	0.020	27.22	9.519	0.69	0.56
66.80	1.902	0.018	28.93	7.842	0.73	0.59
70.51	1.654	0.016	30.65	6.572	0.78	0.58
74.19	1.436	0.010	32.37	5.490	0.42	0.54
77.83	1.278	0.009	34.09	4.692	0.45	0.59
81.43	1.171	0.009	35.81	4.126	0.54	0.55
84.99	1.100	0.009	37.53	3.709	0.56	0.53
88.51	1.055	0.009	39.25	3.401	0.58	0.57

tainty listed in Tables IV(a)–IV(e) (% sys, last column). The total uncertainty (tot) is the quadratic sum of the statistical and systematic uncertainties.

V. DISCUSSION AND RESULTS

Results for the *pp*-elastic-differential cross section are listed in Tables IV(a)–IV(e) and displayed in Figs. 2–6 in comparison with the phase-shift fits (which include the present data) by Arndt *et al.* [47] and Bugg and Bryan [48].

Arndt *et al.* do not fit the shape of the angular distribution, especially near 30° c.m. The fits of Bugg and Bryan, however, are good. In order to see this more clearly, Fig. 7 is plotted as the ratio to fits of the form

$$c_0 + c_2 \cos 2\theta + c_4 \cos 4\theta + c_6 \cos 6\theta,$$

where the coefficients c_0–c_6 are listed in Table V together with the χ^2 per degree of freedom for the fit. The fits to the angular distribution are generally good, with χ^2 per degree of freedom about 1. The phase-shift fits all have χ^2 near 1. The only other data with sufficient accuracy for a meaningful comparison with these angular distributions are those of Hoffmann *et al.* [8], Berdoz *et al.* [33], and Barlett *et al.* [34]. The tables in these papers contain statistical errors only, and so we have included

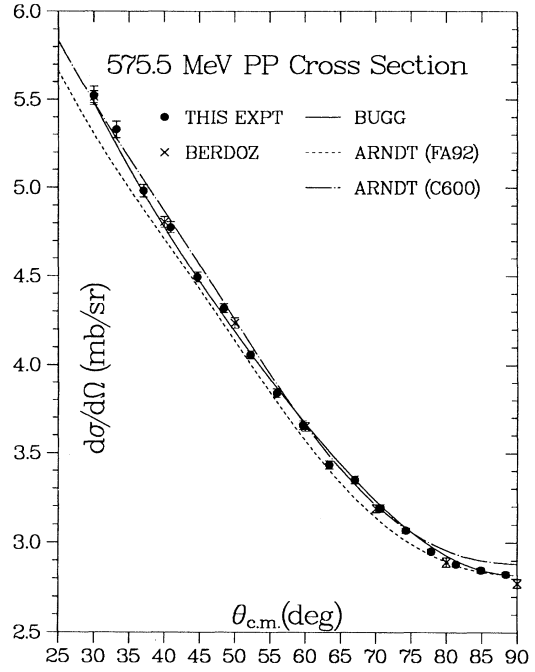

FIG. 3. Differential cross section $d\sigma/d\Omega$ (mb/sr) compared with phase-shift fits by Arndt *et al.* and Bugg and Bryan at 575.5 MeV.

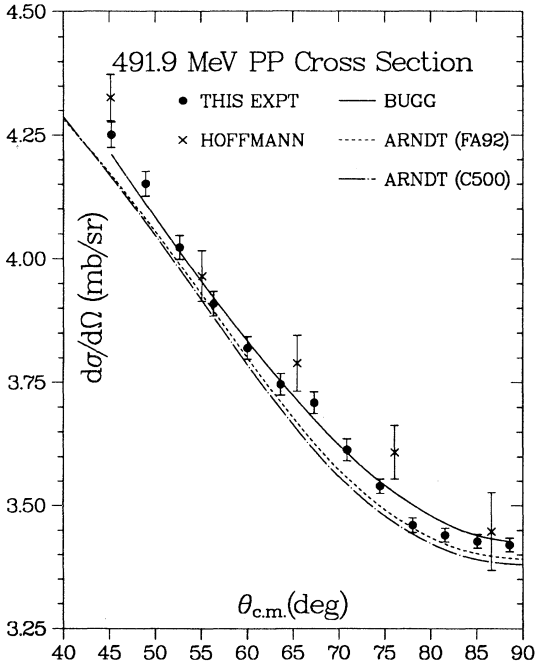

FIG. 2. Differential cross section $d\sigma/d\Omega$ (mb/sr) compared with phase-shift fits by Arndt *et al.* and Bugg and Bryan at 491.9 MeV.

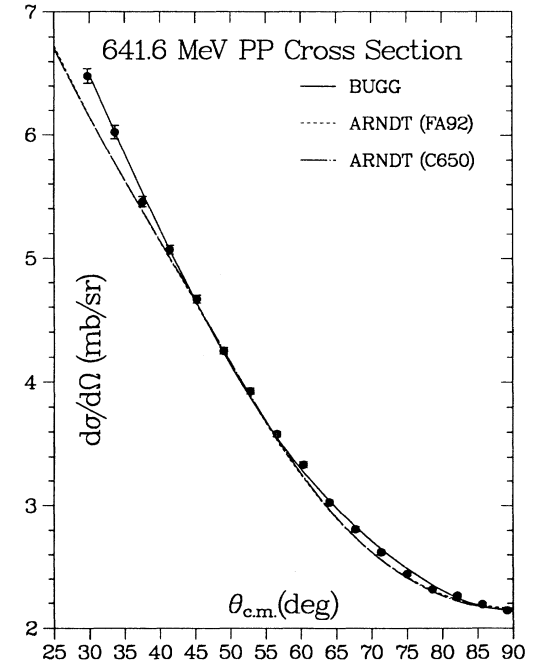

FIG. 4. Differential cross section $d\sigma/d\Omega$ (mb/sr) compared with phase-shift fits by Arndt *et al.* and Bugg and Bryan at 641.6 MeV.

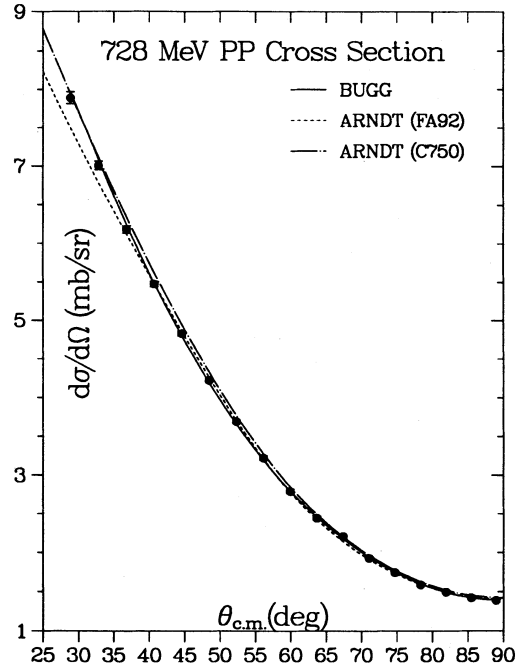

FIG. 5. Differential cross section $d\sigma/d\Omega$ (mb/sr) compared with phase-shift fits by Arndt *et al.* and Bugg and Bryan at 728 MeV.

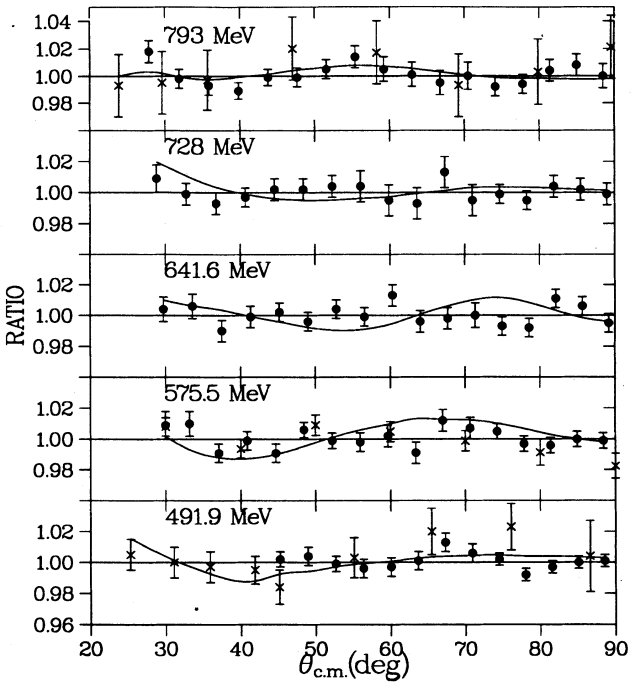

FIG. 7. Angular distributions shown as the ratio of the cross section to the $\cos 2n\theta$ fits defined by Table V. The curve is the phase-shift fit of Bugg and Bryan. The points marked × are from Barlett *et al.* (793 MeV), Berdoz *et al.* (575.5 MeV), and Hoffmann *et al.* (491.9 MeV).

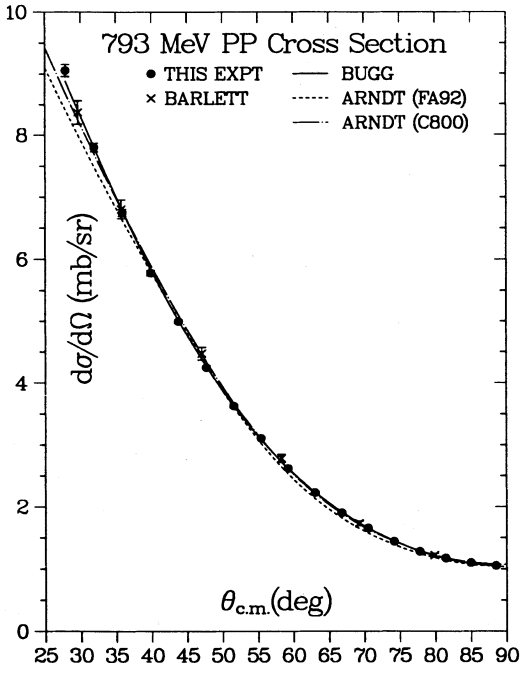

FIG. 6. Differential cross section $d\sigma/d\Omega$ (mb/sr) compared with phase-shift fits by Arndt *et al.* and Bugg and Bryan at 793 MeV.

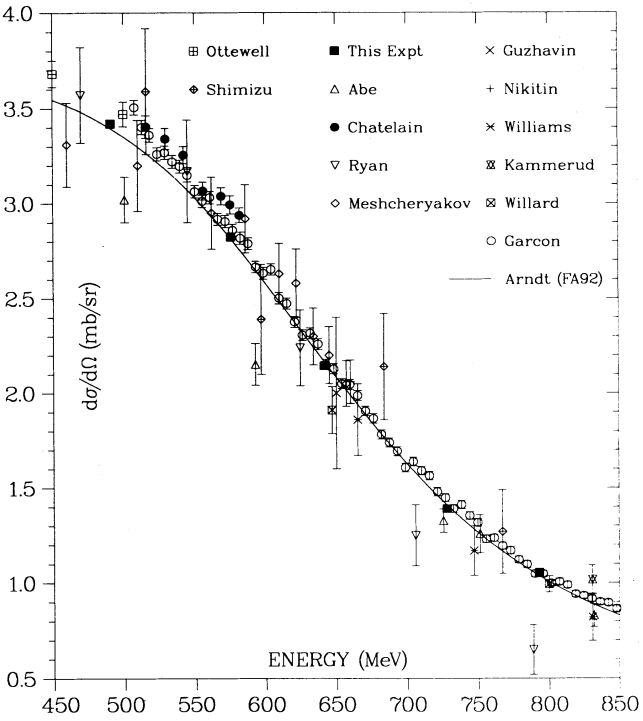

FIG. 8. Differential cross section at 90° c.m. versus beam energy, compared with the FA92 phase-shift solution of Arndt *et al.* and with previous data.

TABLE V. Coefficients of $\cos 2n\theta$ fit $\sigma(\theta) = c_0 + c_2 \cos 2\theta + c_4 \cos 4\theta + c_6 \cos 6\theta$ (mb/sr c.m.) and the χ^2 per degree of freedom for these fits.

MeV	491.9	575.5	641.6	728.2	793.0
C_0	4.248	4.587	5.071	5.630	6.091
C_2	0.832	1.838	3.242	5.011	6.185
C_4	0	0.074	0.395	0.881	1.340
C_6	0	0	0.069	0.109	0.195
χ^2	0.9	1.1	1.1	0.5	1.1

the systematic errors, as discussed in Sec. II C.

Figure 8 shows the absolute normalization of the data in comparison with the phase-shift fit FA92 of Arndt *et al.* [47]. The relative measurements of Garçon *et al.* [6] have been multiplied by 0.98. The data of Chatelain *et al.* [16] are a few percent high, as explained in Sec. II B.

With the inclusion of these new data Bugg and Bryan report stable solutions for the first time near 650 MeV for both isospin-0 and -1 and near 720 MeV for isospin-1 only. Near 800 MeV the phase-shift solutions agree for the first time with precise measurements of the *pp* total cross sections and with reasonable estimates for the *pp* inelastic cross sections [49,50]. The latest phase shifts favor the values of VerWest and Arndt [49] over those of Bystricky *et al.* [50].

Phase-shift analysis averages many discrete measurements into smooth functions. Subject to this limitation, we believe that these new data complete the determination of the isospin-1 amplitudes from 500 to 800 MeV, stabilizing the phase-shift solutions and providing an accurate calibration standard to which other data may be normalized.

ACKNOWLEDGMENTS

We would like to thank Jim Amann for help with the beam counters, Jan Novak, Gary Isom, and the cryogenics crew for building the target, David Lee for the loan of two MWPC's, and David Bugg, Gerry Garvey, and Peter Gram for valuable advice. This work is supported in part by the U.S. Department of Energy Contract No. W-7405-ENG-36, Grants Nos. DE-FG05-88ER40446, DE-FG03-88ER40424, and DE-FG05-88ER40399, and by the National Science Foundation.

[1] J. Bystricky, F. Lehar, and P. Winternitz, J. Phys. **39**, 1 (1978).
[2] M. J. Longo and B. J. Moyer, Phys. Rev. **125**, 701 (1962).
[3] D. V. Bugg *et al.*, Phys. Rev. **146**, 980 (1966).
[4] F. Shimizu, Y. Kubota, H. Koiso, F. Sai, S. Sakamoto, and S. S. Yamamoto, Nucl. Phys. **A386**, 571 (1982).
[5] M. G. Albrow, S. Anderson-Almehed, B. Bosnjakovic, C. Daum, F. C. Erne, J. P. Lagnaux, J. C. Sens, and F. Udo, Nucl. Phys. **B23**, 445 (1970).
[6] M. Garçon, D. LeGrand, R. M. Lombard, B. Mayer, M. Rouger, Y. Terrien, and A. Nakach, Nucl. Phys. **A445**, 669 (1985).
[7] D. Aebischer, B. Favier, L. G. Greenians, R. Hess, A. Junod, C. Lechanoine, J. C. Nikles, D. Rapin, C. Richard-Serre, and D. W. Werren, Phys. Rev. D **13**, 2478 (1976).
[8] G. W. Hoffmann, M. L. Barlett, R. W. Fergerson, J. A. Marshall, J. A. McGill, E. C. Milner, L. Ray, and J. F. Amann, Phys. Rev. C **37**, 397 (1988).
[9] D. Ottewell, P. Walden, E. G. Auld, G. Giles, G. Jones, G. J. Lolos, B. J. McParland, W. Ziegler, and W. Falk, Nucl. Phys. **A412**, 189 (1984).
[10] R. J. Barrett, B. D. Anderson, H. Willard, A. N. Anderson, and N. Jarmie, Nucl. Instrum. Methods **129**, 441 (1975).
[11] H. Willard, B. D. Anderson, H. W. Baer, R. J. Barrett, P. R. Bevington, A. N. Anderson, H. Williams, and N. Jarmie, Phys. Rev. C **14**, 1545 (1976).
[12] A. N. Anderson, Ph.D. thesis, University of Idaho, 1975.
[13] F. Irom, G. J. Igo, J. B. McClelland, and C. A. Whitten, Jr., Phys. Rev. C **25**, 373 (1982).
[14] F. Irom, Ph.D. thesis, UCLA, 1981; Los Alamos Report No. LA-8648-T, 1981.
[15] S. J. Nikitin, J. M. Selector, E. G. Bogomolov, and S. M. Zombkovskij, Nuovo Cimento **2**, 1269 (1955).
[16] P. Chatelain *et al.*, J. Phys. G **8**, 643 (1982).
[17] G. Pauletta, G. Adams, S. M. Haji-saeid, G. J. Igo, J. B. McClelland, A. T. M. Wang, C. A. Whitten, Jr., A. Wreikat, M. M. Gazzaly, and N. Tanaka, Phys. Rev. C **27**, 282 (1983).
[18] F. Shimizu, H. Jiusim, Y. Kubota, F. Sai, S. Sakamoto, and S. S. Yamamoto, Nucl. Phys. **A389**, 445 (1982).
[19] V. M. Guzhavin *et al.*, Zh. Eksp. Teor. Fiz. **47**, 1228 (1964) [Sov. Phys. JETP **20**, 830 (1965)].
[20] R. A. Ryan, A. Kanofsky, T. J. Devlin, R. E. Mischke, and P. F. Shepard, Phys. Rev. D **3**, 1 (1971).
[21] D. T. Williams *et al.*, Nuovo Cimento A **8**, 447 (1972).
[22] R. C. Kammerud, B. B. Brabson, R. R. Crittenden, R. M. Heinz, H. A. Neal, H. W. Paik, and R. A. Sidwell, Phys. Rev. D **4**, 1309 (1971).
[23] K. Abe, B. A. Barnett, J. H. Goldman, A. T. Laasanen, P. H. Steinberg, G. J. Marmer, D. R. Moffett, and E. F. Parker, Phys. Rev. D **12**, 1 (1975).
[24] R. Dubois, D. Axen, R. Keeler, M. Comyn, G. A. Ludgate, J. R. Richardson, N. M. Stewart, A. S. Clough, D. V. Bugg, and J. A. Edgington, Nucl. Phys. **A377**, 554 (1982).
[25] L. W. Smith, A. W. McReynolds, and G. Snow, Phys. Rev. **97**, 1186 (1955).
[26] R. B. Sutton, T. H. Fields, J. G. Fox, J. A. Kane, W. E. Mott, and R. A. Stallwood, Phys. Rev. **97**, 783 (1955).
[27] E. T. Boschitz, W. K. Roberts, J. S. Vincent, M. Blecher, K. Gotow, P. C. Gugelot, C. F. Perdrisat, L. W. Swenson, and J. R. Priest, Phys. Rev. C **6**, 457 (1972).
[28] M. G. Meshcheryakov, B. S. Neganov, L. M. Soroko, and J. K. Vzorov, Dokl. Akad. Nauk SSSR **99**, 959 (1954).
[29] G. N. Velichko, A. A. Vorob'ev, Y. K. Zalite, G. A. Korolev, E. M. Maev, N. K. Terent'ev, A. V. Khanzadeev, and V. A. Shchegel'skil, Yad. Fiz. **35**, 1457 (1982) [Sov. J. Nucl. Phys. **35**, 852 (1982)].
[30] A. V. Dobrovolsky *et al.*, Nucl. Phys. **B214**, 1 (1983).
[31] E. Gülmez *et al.*, Nucl. Instrum. Methods A **297**, 7

(1990).
[32] E. Gülmez and C. A. Whitten, Jr., Nucl. Instrum. Methods A **297**, 17 (1990).
[33] A. Berdoz, B. Favier, F. Foroughi, J. Hoftiezer, G. S. Mutchler, and Ch. Weddigen, J. Phys. G **8**, 1363 (1982).
[34] M. L. Barlett *et al.*, Phys. Rev. C **27**, 682 (1983).
[35] P. R. Bevington *et al.*, Phys. Rev. Lett. **41**, 384 (1978).
[36] M. W. McNaughton, P. R. Bevington, H. B. Willard, E. Winkelmann, E. P. Chamberlin, F. H. Cverna, N. S. P. King, and H. Willmes, Phys. Rev. C **23**, 1128 (1981).
[37] D. W. MacArthur, K. B. Butterfield, D. A. Clark, J. B. Donahue, P. A. M. Gram, H. C. Bryant, C. J. Harvey, W. W. Smith, and G. Comtet, Phys. Rev. Lett. **56**, 282 (1986).
[38] A. H. Mohagheghi, Ph.D. thesis, University of New Mexico, 1990; Los Alamos Report No. LA-11925-T, 1990.
[39] L. Ray, Phys. Rev. C **20**, 1857 (1979).
[40] A. J. Simon, Ph.D. thesis, Texas A&M, 1993.
[41] E. Gülmez *et al.*, Phys. Rev. C **43**, 2067 (1991).
[42] E. Gülmez *et al.*, Nucl. Phys. **A551**, 621 (1993).
[43] D. W. Werren *et al.*, Los Alamos Report No. LA-5396-MS, 1973.
[44] D. Brown, Nucl. Instrum. Methods **117**, 561 (1974).
[45] B. Sundqvist, L. Glantz, A. Johansson, L. Amtén, and I. Koersner, Nucl. Instrum. Methods **153**, 301 (1978).
[46] P. U. Renberg *et al.*, Nucl. Instrum. Methods **104**, 157 (1972).
[47] R. A. Arndt, L. D. Roper, R. L. Workman, and M. W. McNaughton, Phys. Rev. D **45**, 3995 (1992).
[48] D. V. Bugg and R. A. Bryan, Nucl. Phys. **A540**, 449 (1992).
[49] B. VerWest and R. A. Arndt, Phys. Rev. C **25**, 1979 (1982).
[50] J. Bystricky, P. LaFrance, F. Lehar, F. Perot, T. Siemiarczuk, and P. Winternitz, J. Phys. (Paris) **48**, 1901 (1987).